Advances in Water Resources 160 (2022) 104118

Contents lists available at ScienceDirect

Advances in Water Resources

journal homepage: www.elsevier.com/locate/advwatres

Joint estimation of groundwater salinity and hydrogeological parameters using variable-density groundwater flow, salt transport modelling and airborne electromagnetic surveys

Jude King [a,b,*], Tobias Mulder [a], Gualbert Oude Essink [a,b], Marc.F.P. Bierkens [a,b]

[a] Utrecht University, Department of Physical Geography, Utrecht, the Netherlands
[b] Deltares, Utrecht, the Netherlands

A B S T R A C T

Freshwater aquifers in low elevation coastal zones are known to be threatened by saltwater intrusion (SWI). As these areas host a significant share of the world's population, an excellent understanding of this phenomenon is required to effectively manage the availability of freshwater. SWI is a dynamic process, therefore saline groundwater distributions can change quickly over time – particularly in stressed areas with anthropogenic drivers. To model these changes, regional 3D variable-density groundwater (3D-VDG) flow and coupled salt transport models are often used to estimate the current (and future distributions) of saline groundwater. Unfortunately, parameterising 3D-VDG models is a challenging task with many uncertainties. Generally, uncertainty is reduced through the addition of observational data – such as Airborne Electromagnetic (AEM) surveys or ground-based information – that offer information about parameters such as salinity and hydraulic head. Recent research has shown the ability of AEM surveys to provide accurate 3D groundwater salinity models across regional scales, as well as highlighting the potential for good survey repeatability. To this end we investigated the novel approach of using repeat AEM surveys (flown over the same area at different points in time) and 3D-VDG models to jointly improve the parameterisation of 3D-VDG models - while simultaneously providing a detailed 3D map of groundwater salinity distributions. Using detailed 3D synthetic models, the results of this study quantitatively highlight the usefulness of this approach, while offering practical information on implementation and further research.

1. Introduction

3D variable-density groundwater flow and coupled salt transport models – referred to in the following as 3D-VDG models – are proven and commonly used tools to simulate current and future distributions of saline groundwater (e.g. Faneca Sànchez et al., 2012; Meyer et al., 2019; Van Engelen et al., 2019). The usefulness of 3D-VDG models is particularly clear in highly populated low elevation coastal zones, where saltwater intrusion (SWI) into freshwater groundwater systems poses a significant risk to the availability of fresh water for agricultural, industrial and household uses (Gomaa et al., 2021; Oude Essink et al., 2010; Simmons et al., 2010; Werner et al., 2013). As a result, 3D-VDG models are extensively used to inform groundwater policies in these areas.

The parameterization of 3D-VDG models, i.e., finding values for ground water flow (e.g., hydraulic conductivity, storage coefficients) and salt transport (e.g., porosity, dispersivities) parameters is a daunting task. Particularly as these parameters can be very heterogeneous in space. Typically, the parameterization process starts with a hypothesis about parameter heterogeneity. This is followed by creating a spatial regionalization (e.g., zonation, geostatistical simulation) which reduces the number of free (unknown) parameters. Next, following an initial guess, the free parameters are estimated through model calibration. Calibration is often approached as an inverse problem, where model parameters are iteratively adjusted until the model response fits to observations of models states or outputs. For an overview of calibration approaches we refer to Zhou et al. (2014) and Doherty (2010), for an example of an application to 3D-VDG models refer to Carrera et al. (2010). Typically, 3D-VDG models are calibrated using in-situ head and salinity observations which are often sparse. Adjusted 3D-VDG parameters include, for example, hydraulic conductivity, porosity, dispersivity and recharge. However, 3D-VDG parameterization is prone to uncertainty. First, the large spatial heterogeneity of underground lithology creates errors during the spatial regionalization step. Second, calibration being an inverse problem usually suffers from non-uniqueness as a result of parameter correlation (Carrera et al., 2005), which arises from the sparseness of the in-situ observation used.

Naturally, one way to reduce uncertainty is the addition of more observational data that relate to observing 3D-VDG states (head, salinity) or outputs (e.g., stream discharge and concentration). Data sources are often ground-based, such as wells that monitor salinity and

* Corresponding author.
E-mail address: judeking012@gmail.com (J. King).

https://doi.org/10.1016/j.advwatres.2021.104118
Received 11 August 2021; Received in revised form 23 December 2021; Accepted 24 December 2021
Available online 26 December 2021

hydraulic head, or indirect geophysical methods such as Electrical Resistivity Tomography that measure electrical conductivity (EC) (Beaujean et al., 2014) which is converted to groundwater salinity estimates using petrophysical relationships. For regional 3D-VDG modelling, often extending across 100′s of kms (e.g. Cobaner et al., 2012; Gossel et al., 2010; Mabrouk et al., 2019; Michael et al., 2009; Nocchi and Salleolini, 2013; Oude Essink et al., 2010; Van Engelen et al., 2019), 1D or 2D ground measurements are considered expensive – offering localized and disconnected information (King et al., 2020). Airborne Electromagnetics (AEM) offer an indirect, but fast and economical data source to overcome these shortcomings.

The AEM method is sensitive to both lithology and groundwater, where primarily clay content and groundwater salinity offer electrical conductivity (EC) contrasts (Revil and Glover, 1998). As a result, the use of AEM to resolve state variables, such as groundwater salinity, and parameters has proliferated in recent years. AEM methods have been used successfully to map structure such as clay content or lithological units (Auken et al., 2008; Foged et al., 2014; Gunnink et al., 2012; Høyer et al., 2015) and such could be used to help parameterize 3D-VDG models with additional lithological information. In more saline environments however, mapping structure (which can relate to parameters such as hydraulic conductivity) is more challenging because signals are dominated by the strong EC contrasts found at fresh-saline interfaces (King et al., 2020). Naturally, this makes it highly suitable for mapping salinity instead, where in these environments the method has seen continued success for decades (Delsman et al., 2018; Faneca Sànchez et al., 2012; Fitterman and Deszcz-Pan, 2001; Jørgensen et al., 2012; Rahman et al., 2021; Vandevelde et al., 2018).

Conceptually, calibrating a 3D-VDG model with state variables obtained from geophysical data can be approached using sequential or coupled hydrogeophysical inversion (Herckenrath et al., 2013; Hinnell et al., 2010). For an overview and history of hydrogeophysical methods see Binley et al. (2015). In sequential methods a deterministic geophysical inversion is traditionally run first, and then translated into groundwater salinity using petrophysical relationships – allowing model calibration (e.g. Faneca Sànchez et al., 2012). Coupled hydrogeophysical inversion involves the transformation of 3D-VDG state variables into a physical property which can then be forward modelled and compared to geophysical observations (e.g. Bauer-gottwein et al., 2010; González-Quirós and Comte, 2021; Steklova and Haber, 2015). As a result, coupled models do not rely on a geophysical inversion. The 3D-VDG model can then be run iteratively until a misfit against geophysical observations are appropriately small.

In the following we present a method that exploits the ability of AEM to map groundwater salinity to improve the parameterization of 3D-VDG model properties, while at the same time providing improved 3D-VDG predictions of groundwater salinity. We use the idea that the distribution of saline and fresh groundwater changes over time and the resulting movement of EC contrasts between fresh and saline groundwater can be resolved by AEM if measured repeatedly at the same location. Furthermore, previous research suggests that if repeated flightline paths are spatially consistent and that inverted data are compared, rather than the electromagnetic response itself, then the AEM method offers good repeatability (Huang and Cogbill, 2006).

Thus, using a similar idea to traditional inverse calibration, where a model is run from the past to match observations at the present, we explore the possibility of using two separate AEM surveys flown at the same location at two different periods in time. Similar to time-lapse inversion that has been used extensively in reservoir engineering (Johnston, 2013) and hydrology (e.g. Karaoulis et al., 2011), we investigate the idea that the observed changes in salinity distributions can infer model 3D-VDG parameters. If a 3D-VDG model with initial groundwater salinity distributions obtained from the first survey, say at t_0, it should be able to predict the groundwater salinity distribution at the time of the second AEM survey (say t_1).

Given that groundwater in the Netherlands is generally a mixture of seawater and freshwater, chloride is the dominant conservative anion, therefore for consistency we will refer to a distribution of groundwater salinity as the chloride distribution. To test the idea and to see if such inverse estimation would be feasible in theory, we created a highly detailed synthetic reality (3D lithology and chloride distribution over time between t_0 and t_1) based on real AEM data (Delsman et al., 2018), a detailed lithological model (Stafleu et al., 2011) and 3D-VDG modelling with the computer code SEAWAT (Langevin et al., 2007; Verkaik et al., 2021) and a given set of "real" parameters. We then used a geophysical modelling approach (King et al., 2020) to simulate an AEM survey at the start and end of the 3D-VDG model run. We subsequently tested an optimization strategy that iteratively runs the 3D-VDG model with unknown parameters between t_0 and t_1 while comparing this "modelled" chloride distribution with the AEM survey at t_1 and adjust the unknown 3D-VDG model hydrogeological parameters to minimize the difference. Using this approach, it was tested if the original "real" parameters could be re-estimated correctly.

In the following we provide a summary of our approach in Section 3.1. Section 3.2 describes how the synthetic model was created including the study area it was based on, followed by the 3D-VDG model set up and parameterization in 3.3 and the optimization method in 3.4. Section 4 outlines the results of the optimization, which are followed a discussion and finally concluding remarks in 5 and 6 respectively.

2. Methods

2.1. General approach

Our approach to estimate hydrogeological parameters is based on performing two sequentially processed AEM surveys, one at time t_0 and one at time t_1, that are sufficiently spaced apart to detect real changes in the chloride distribution of a groundwater body. This means that the approach is limited to groundwater systems where due to external forcing (extraction fresh groundwater, injecting fresh water, sea-level rise) the chloride distribution changes relatively rapidly. The estimated chloride distribution obtained from the survey at time t_0 is used as initial condition by a 3D-VDG model that is subsequently used to simulate the chloride distribution at time t_1. This simulation is first done with an initial estimate of the unknown hydrogeological parameters. We then perform a simulated AEM survey on the 3D-VDG model simulated chloride distribution to obtain an AEM chloride distribution at the same (lower) spatial footprint as the actual AEM survey at t_1 (see Fig. 2). The differences between the actual and simulated AEM chloride distributions are then used to drive an optimization framework, as outlined in Fig. 1. Here, the unknown hydrogeological parameters are adjusted. The 3D-VDG model and AEM simulation and parameter estimation steps are repeated iteratively while minimizing the differences between the actual and simulated AEM at t_1. In effect, we are applying a coupled, optimization driven time-lapse hydrogeophysical inversion. The result of this approach are optimized estimates of the unknown hydrogeological parameters and an optimized estimate of the chloride distribution at the resolution of the 3D-VDG model (generally higher than that of an AEM survey) which is also consistent with physical laws.

At the moment, to our knowledge, regional-scale time-lapse AEM surveys are non-existent, but to be expected in the near future. Thus, to demonstrate the methodology, we used a so-called twin-experiment where we use a realistic synthetic reality and simulated AEM surveys. The complete setup of the twin experiment is shown in Fig. 1a) the synthetic reality which consists of a realistic chloride distribution at t_0 and t_1 simulated with the 3D-VDG model using the "real hydrogeological parameters" and two simulated AEM surveys (in blue); b) the model simulation (also using the 3D-VDG model) and 3D-VDG model based AEM survey used in the optimization (light blue); and c) the optimization algorithm (orange). We note that the simulated AEM surveys include realistic observation noise and degrading of resolution conform the AEM footprints (King et al., 2020). Using the same 3D-VDG

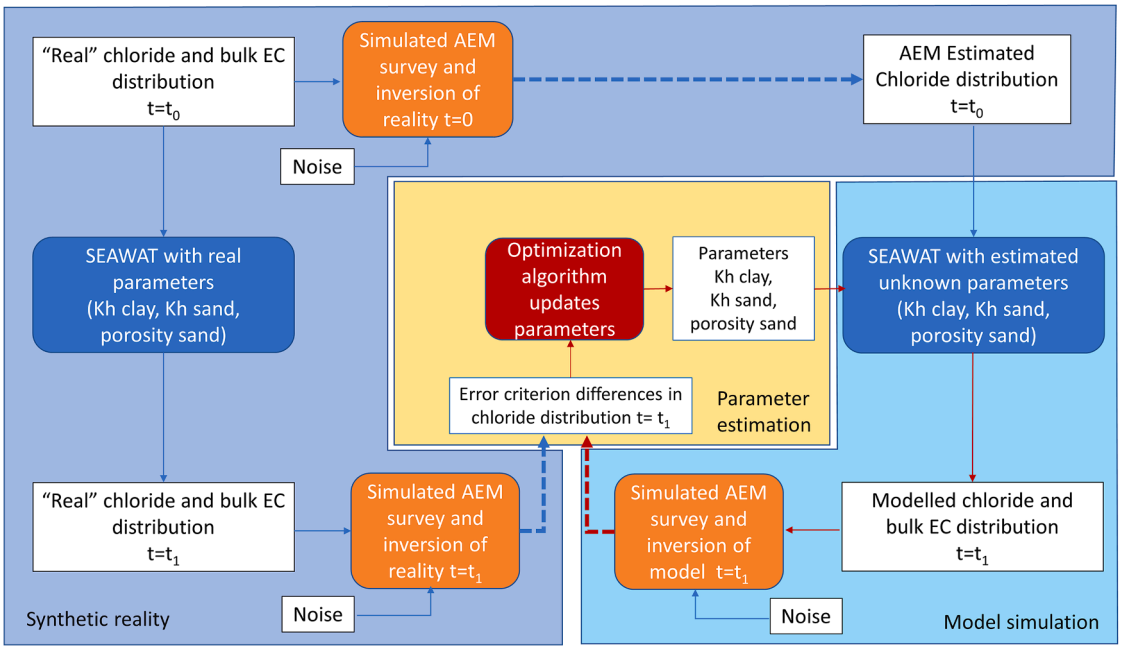

Fig. 1. Method outline. Dark blue region (left): creating the synthetic reality, light blue region (right): iterating over simulated models with given parameters, yellow region (centre): estimating subsurface parameters. White squares: 'real' 3D chloride distributions in time, orange squares: geophysical simulations of 'real' 3D chloride distributions, blue squares: 3D-VDG model run with given parameters, red square: parameterization update (driven by optimization strategy). Dashed lines indicate a petrophysical transformation from inverted ECb to chloride.

model for reality and model simulation means that we ignore model structural errors.

In the following we describe in more detail: a) the synthetic case, including the simulated AEM in Section 2.2; b) the model simulation and initial hydrogeological parameter estimates in Section 2.3; c) optimization routine in Section 2.4.

2.2. Creating a synthetic case

The synthetic case was generated from 3D estimates from an existing AEM survey from the Province of Zeeland in The Netherlands (Delsman et al., 2018). Within this region, data was extracted from an area called Zeeuws-Vlaanderen (or Zeelandic Flanders in English), in southern

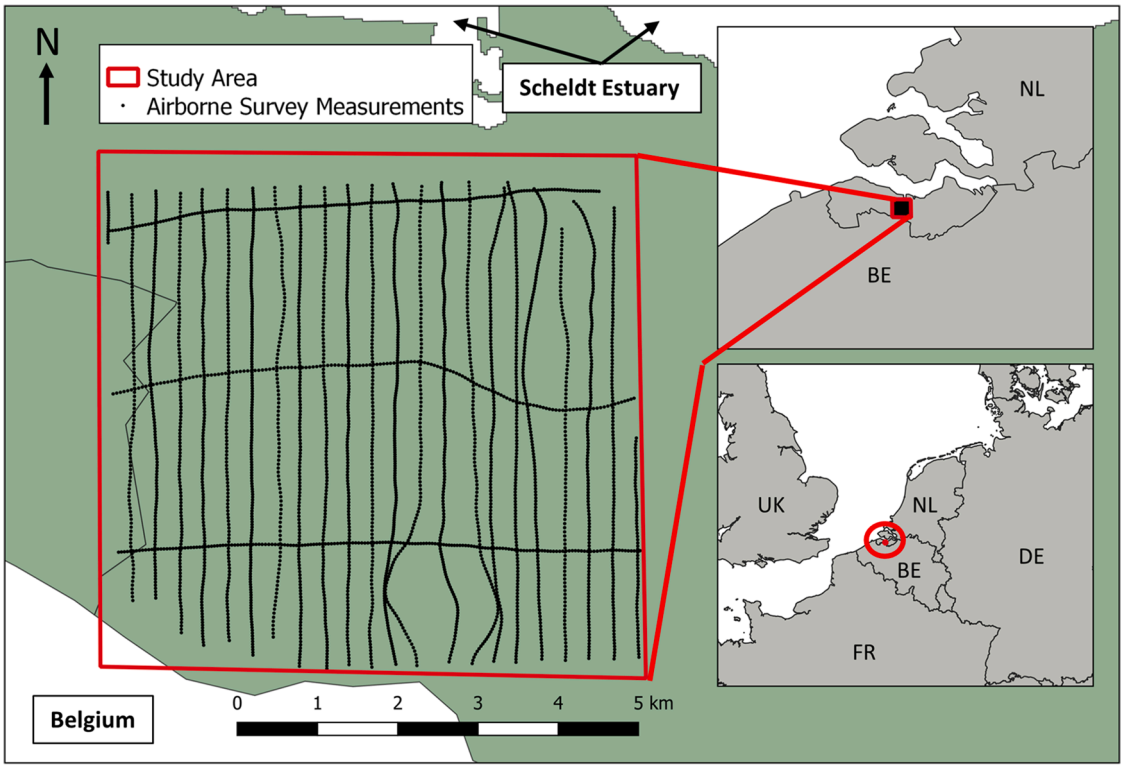

Fig. 2. Location of the case study used to create the synthetic case. The flight lines shown are the same as in the original AEM survey.

Zeeland. This east-west orientated strip (~60 × 15 km) is bordered to the North by the Scheldt River estuary and to the south by the Belgian border. At the centre of Zeeuws-Vlaanderen, around the town of Terneuzen, a subset area was selected covering ~7 × 7 km for further processing. The model area and AEM flightlines are highlighted in Fig. 2.

The groundwater system characteristics of the area are summarized by the presence of shallow freshwater lenses typically about 10 – 20 m thick (Delsman et al., 2018), caused by Holocene sea-level transgressions and subsequent land reclamation (Berendsen, 2005; Delsman et al., 2014). The hydrogeological system is hosted within lithologies comprising Neogene and Quaternary sediments (Stafleu et al., 2011), including younger fine sands, clays and peats, with deeper northward dipping sand and silts (Vos, 2015). Within the study area, the dipping hydrogeological base extends to ~50 – 70 m below the surface and denotes an impermeable aquitard. To create a synthetic reality, we use the existing detailed 3D chloride distribution that was obtained from the AEM survey performed over the Province of Zeeland (Delsman et al., 2018). This chloride distribution was taken as the "real chloride distribution" at t_0. For this area, a very detailed 3D-lithological characterization is available (Stafleu et al., 2011), based on ~1500 borelogs in the study area (see Fig. 3). In our synthetic example, we assume the lithology to be fully known and focus on estimating the chloride distribution and hydrogeological parameters only.

2.2.1. *Translation of chloride to electrical conductivity*

The chloride distribution and lithological information were further processed into bulk electrical conductivity (ECb) to allow for the simulation of an AEM survey and subsequent inversion. First, a known empirical relationship from the study area was used to transform the data into the electrical conductivity of the groundwater (ECw) and corrected from a reference groundwater temperature of 25 °C to 11 °C, as outlined in P.G.B. De Louw et al. (2011). As the ECb is a product of both lithology and pore water salinity, a petrophysical transformation is required to split the information between the two. The simplest approach is using apparent formation factors (FF) which are the ratio of saturated sediment (ECb) to that of the pore water itself (ECw) (Archie,

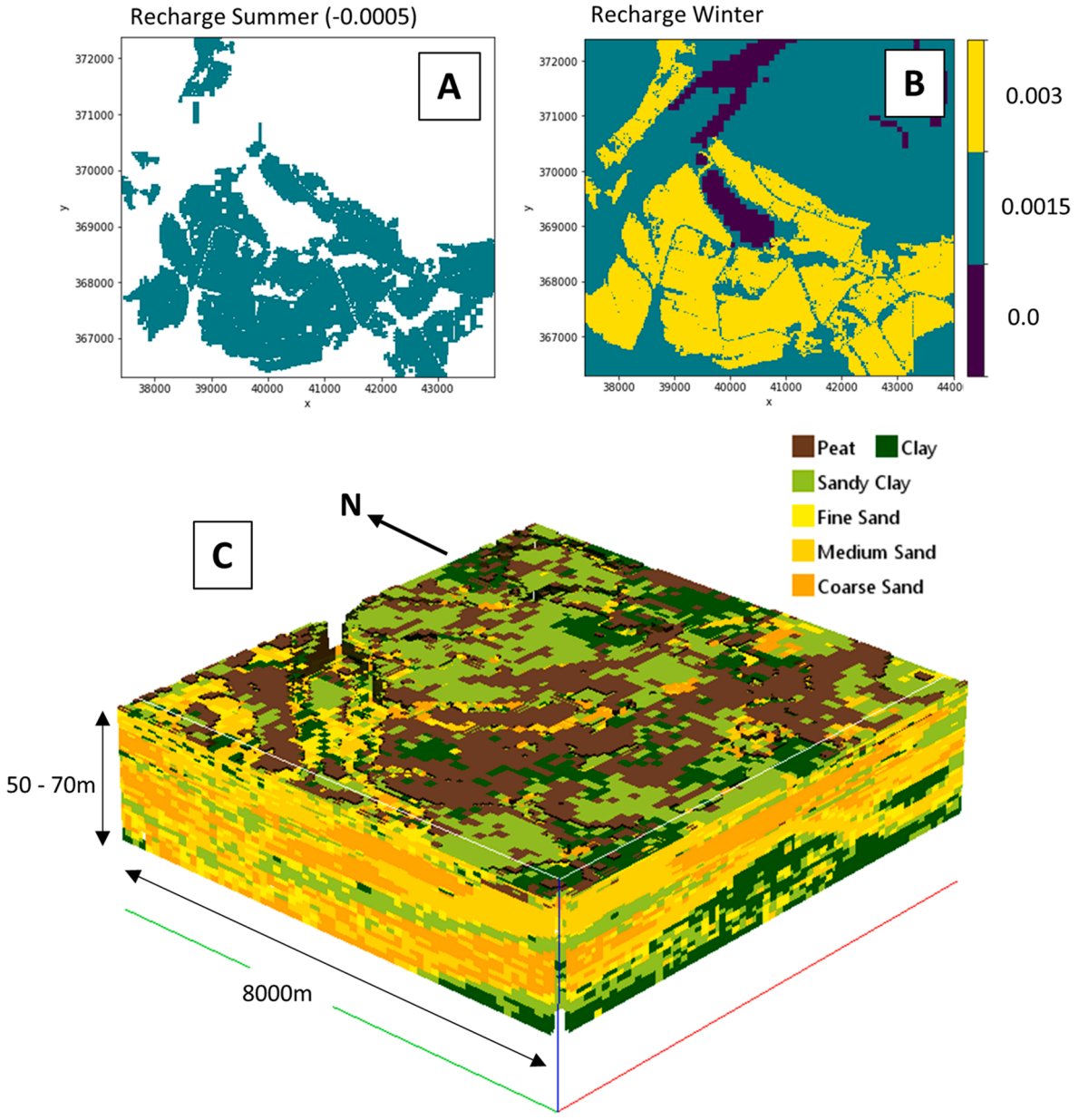

Fig. 3. 3D-VDG model set up highlighting areas of extraction, represented as summer recharge (A) with enhanced recharge in the extraction areas (B), both as m/day. The lithological model (C) that was used to assign hydraulic conductivities, shown with 25 x vertical exaggeration.

Table 1
Formation factors used per sediment class for the conversion of ECb data to chloride.

Lithology	Formation factor (FF)	Std	Samples
Peat	2.1	0.7	41
Clay	2.5	0.6	192
Sandy clay	2.8	0.8	52
Fine sand	3.2	0.4	299
Medium sand*	4		
Coarse sand*	5		

*FF taken from another study (Goes et al., 2009), without uncertainty and sample numbers.

1942). The electrical properties of clays minerals such as surface conductivity complicate this relationship (Revil et al., 2017). As a result, a more accurate transformation in areas with clay present requires the addition of surface conductivity, such as Waxman and Smits (2003). In this study we decided to use the simpler, apparent FFs (ECb/ECw) – values are shown in Table 1. The values for apparent FFs were taken from over 500 samples in an area only 20 km away from the area that was used to create our synthetic model, and therefore offered good representative values.

The 3D distribution of lithological units to derive the FF distribution is the one taken from GeoTOP (Stafleu et al., 2011) (Fig. 3) and corresponding FF values from nearby field-measurements, as shown in table 1. (P.G.B. De Louw et al., 2011).

2.2.2. Obtaining the chloride distribution at t_1 using a 3D-VDG model

To set up a 3D-VDG model that produces a realistic change in chloride distributions at t_1, we constructed a model that comprises a combination of typical anthropogenic and natural drivers that result in chloride movements – while at the same time ensuring that the model changes enough to produce sufficient signal. Natural drivers are natural recharge and autonomous freshening and salinization that occurs as a result of past inundation or sea level change (Vos, 2015). We also introduced anthropogenic drivers: extensive groundwater extraction that results in the so-called upconing (or shallowing) of brackish to saline groundwater and areas with enhanced recharge of fresh surface water through Aquifer Storage and Recovery (ASR) (Dillon, 2005), which would likely result in a rapid increase of fresh groundwater volumes (Pauw et al., 2015; Zuurbier et al., 2015).

With this in mind, a 3D-VDG model was discretized into 25 × 25 m horizontal cells across a ~8 × 8 km area and comprised a 0.5 m vertical resolution at shallow depths, increasing in thickness logarithmically with depth to a maximum thickness of 10 m, resulting ~3.5 million active cells over 54 layers. A hydrogeological base was assigned at between 50 and 70 m depth and was derived from the GeoTOP model and REGIS (Vernes et al., 2010). The hydrogeological parameters of the model were similarly taken from the 3D lithology distribution of GeoTOP, assigning the parameter values from Table 2. Here, lithology classes coarse, medium, fine loamy and silty sand were assumed as aquifer material and the finer and organic classes as aquitard material. Well locations were selected based on three conditions, in all model cells that are: (1) at 8 m depth (below surface), (2) within aquifer lithologies, and (3) within freshwater areas (<0.5 g/l chloride).

To understand how an AEM survey might respond to groundwater chloride movements across a broad range of time-scales, the model was run for 60 years, longer than was thought necessary for this study. Finally, at every consecutive 6 month time-step, we modelled the geophysical response of the AEM system. In this study, we conclude that after 15 years there was likely sufficient signal available for the AEM system based on a known noise threshold of 5%, (see the Results section).

Table 2
The parameters chosen for the 3D-VDG model.

Parameter	Description	Value (unit)
K_h Aquifer	*Horizontal hydraulic conductivity of the aquifer (m/day)*	10 (m/day)
K_h Aquitard	*Horizontal hydraulic conductivity of the aquitard (m/day)*	0.01 (m/day)
K_h/K_v	*Anisotropy*	3.3 (aquifer) 2 (aquitard)
Porosity	*Porosity*	35 (%)
Recharge winter	*Recharge in winter, higher values denote ASR areas*	0.003 m/day (ASR areas), 0.0015 m/day (other areas)
Recharge summer	*Recharge in summer, negative value denotes evaporation*	−0.0005 m/day
Well Extraction winter	*Groundwater extraction in winter*	0 m^3/day per model cell
Well Extraction summer	*Groundwater extraction in summer*	−0.625 m^3/day per model cell

2.2.3. Simulating an AEM survey

As highlighted in Fig. 1, to recover a 3D chloride distribution that has the same resolution and physical characteristics of an actual survey at t_0 and t_1, an AEM survey needed to be simulated. The process is similar to (King et al., 2020) and is summarized in the following. Existing measurement locations and flightlines (typically with a spacing between 30 and 60 m) were taken from the survey that produced the "real" 3D chloride distribution (Section 2.2.1). ECb values, which are obtained using the method explained in Section 2.2.1, were then sampled at these points every ~50 m to facilitate fast inversion times while still honouring the 50 m horizontal resolution of the 3D model. Vertical sampling was done at 0.5 m intervals. The horizontal resolution, or footprint of the system, is approximated as a 100 – 200 m diameter circles directly beneath the towed instrument (Reid et al., 2006; Yin et al., 2014). Therefore, at each measurement location, the nearest two model cells were averaged to imitate a 100 m footprint. Data were forward modelled using AarhusINV (Auken et al., 2005). Coil source and receiver spacing, and orientations were selected based on the values used by Fugro's RESOLVE HEM system during the original survey (Delsman et al., 2018). Finally, to approximate the noise levels present during FEM acquisition (Farquharson et al., 2003; Green and Lane, 2013), 5% white noise was added to the forward modelled data.

To recover a distribution of electrical properties from an AEM survey, a geophysical inversion is typically undertaken. For this study, a deterministic geophysical inversion (e.g., Auken et al., 2015; Farquharson et al., 2003; Viezzoli et al., 2009; Vignoli et al., 2015) (referred to in the following as an inversion) using AarhusINV (Auken et al., 2015) was implemented. This inversion approach uses a pseudo-2D laterally constrained approach where neighbouring observations are constrained in the regularization process, helping to produce laterally coherent results. The method has been successfully used in many hydrogeophysical studies (e.g. Auken et al., 2008; Chongo et al., 2015; Delsman et al., 2018; Kirkegaard et al., 2011) and is particularly useful in areas with laterally continuous EC contrasts such as our study area.

The inversion starting model consisted of 20 fixed layers, with the first set to 0.5 m thick, increasing logarithmically till 50 m. Below this,

Table 3
Initial parameter estimates used in the first iteration.

Parameter	Initial Estimate (m/day)	Actual Value (m/day)
K_h Aquifer	1	10
K_v Aquifer	0.3	3
K_h Aquitard	0.001	0.01
K_v Aquitard	0.0005	0.005
Effective porosity	0.1	0.35

the final layer is assumed to extend infinitely. Given the highly saline environment, the model was assigned a starting ECb value of 1 S/m. The lateral and vertical constraint parameters were set to 1.3 and 3 respectively, following recommended and commonly used values (Auken et al., 2005). This minimum-structure style inversion changes ECb only and has been found to accurately reproduce smoothly varying chloride distributions (King et al., 2018). The depth of investigation (DOI) varies according to the EC of the subsurface; in this case by shallow saline areas, and therefore could range from ~5 to 60 m in saline or fresh groundwater areas, respectively. The inversion output has an estimation of DOI for each 1D model location. The method to calculate this procedure is described in Vest Christiansen and Auken (2012). All inversions converged to a misfit of less than 5%, thereby effectively explaining the forward modelled observations.

Finally, as a 3D initial groundwater chloride distribution is required for the 3D-VDG model and the inversion method only produces 1D vertical profiles along flightlines, a 3D interpolation step was required. This was approached using a simple method that exploits the layered nature of the inverted data to efficiently produce 3D ECb models from the inversion results. Each one of the 20 inversion layers for all flightlines were interpolated separately using 2D kriging with automatic variogram modelling. The resulting 2D layers were then compiled to produce a 3D model. The method is described in (King et al., 2018) and has been shown to accurately produce 3D volumes of ECb in similar settings. As a final step, the DOI estimates were interpolated using the same 2D Kriging technique, where ECb values below the DOI were filled to the model base using the last encountered ECb value at that depth. Finally, the resulting ECb volume was transformed back into chloride using the reverse of the approach described in Section 2.2a, resulting in simulated AEM surveyed chloride distributions at t_0 and t_1.

2.3. 3D-VDG model simulation and initial parameter estimates

The 3D-VDG model simulation was run iteratively for a 15-year period using the exact same discretization and general parameterization as the model described in Section 2.2.2, except for the unknown parameters. Following extensive experimentation, we conclude that the method was to be used to predict the hydraulic conductivities of the aquifer and aquitard, and porosity. The reasoning behind this choice was two-fold: (1) it was found that the 3D-VDG model was most sensitive to these parameters, and (2) we had to restrict the number of parameters to avoid excessive computation times and identification issues. The ratio of horizontal to vertical conductivity K_h/K_v was kept constant, and thus in effect the optimization was used to resolve three parameters. As this study is unique and therefore a proof of concept, it was felt that while more parameters could be possible, it was important to keep the approach simple. Given that especially higher K_h and K_v values result in longer SEAWAT runtimes, initial estimates were chosen to be too low on purpose to facilitate faster iteration times early on. To test the sensitivity of the optimization to incorrect initial estimates, the starting values were chosen to be ten-times greater than the actual values. Effective porosity was simply assigned by a random guess to test the general robustness of the method. Values used are highlighted in Table 3.

2.4. The optimization

We used a suitable non-gradient global optimizer that works well in the high-dimensional problems typically found in the field of groundwater modelling. For this, the Nelder-Mead downhill-simplex method was selected for its robustness and proven ability to optimize model parameters and find global minima (Nelder and Mead, 1965). Its ability to handle noise is also desirable given the inherent noisiness related to the acquisition of AEM data. The optimization was implemented using the SciPy Optimize package available in Python, that uses an improvement to the original method by adjusting the simplex parameters relative to the dimensionality of the problem (Gao and Han, 2012).

The objective function returns the root mean squared error (RMSE) between t_1 survey and t_1 predicted, given by:

$$RMSE = \sqrt{\frac{\sum_{i=1}^{N}\left(y_{pred,i} - y_{ref,i}\right)^2}{N}} \quad (1)$$

where *pred* at t_1 denote simulated AEM surveyed chloride values based on the 3D-VDG model predictions (with unknown parameters) and *ref* at t_1 the simulated AEM surveyed chloride values based on the synthetic reality (3D-VDG model with known parameters). This was minimized until a convergence criterion was met, in this case given by the RMSE between iterations. This value was set to 0.1 g/l chloride and was chosen to be unrealistically low which effectively allowed the optimization to run indefinitely to allow a user-based decision on whether it has converged sufficiently. In practice, the convergence criteria could however be set to reflect the levels of noise from the AEM system if known.

3. Results

3.1. AEM sensitivity to estimated chloride distributions

The 3D-VDG model was first run for 60 years to understand the length of time needed for chloride changes to be detected by the AEM system at each time-step, and indeed the sensitivity of the AEM method to the transient effects in general. To understand this quantitatively, each time step of the resulting 3D-VDG model was geophysically forward modelled using the method outlined in Section 2, where successive time-steps were compared quantitatively to the first model as relative mean absolute error (%). The 5% red horizontal line in Fig. 4 represents an approximation of AEM noise levels thereby providing a rough indication of required groundwater chloride movements before there is enough signal for a second survey to measure meaningful differences.

From Fig. 4, it follows that prior to ~5 years a repeat survey would likely fall within the estimated noise range, indicating that a repeat survey in this instance would fail to effectively map differences. After 15 years (or 30 time-steps) the slope gradient decreases after an initial sharp increase to ~7.5% difference. Therefore, in the following the time-period between zero and 15 years was used to simulate the two surveys and ultimately guide the optimization. In a real setting, localized ground measurements over time and geophysical forward modelling could be

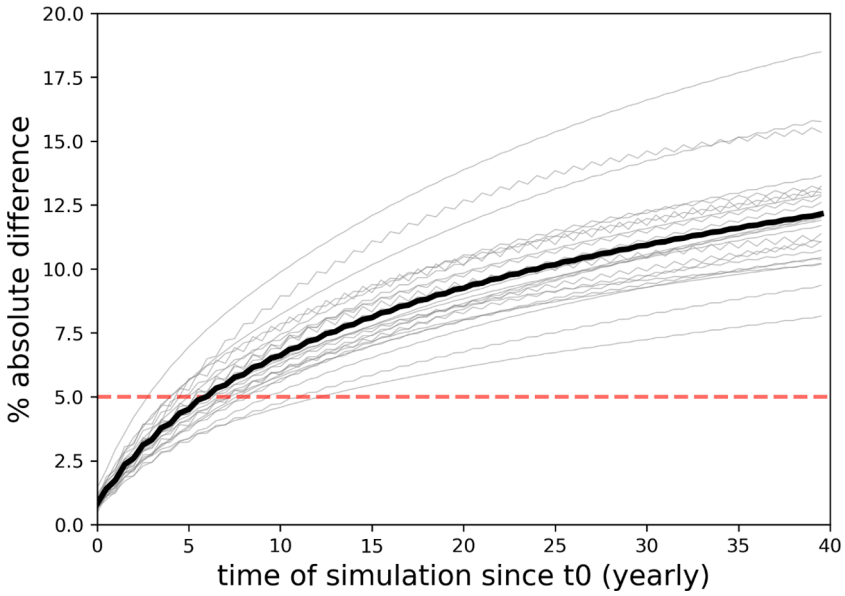

Fig. 4. Sensitivity of the AEM system over time, represented per flightline (light grey lines) and averaged across all flightlines (red line). Sensitivities are represented as the mean absolute difference of all five frequencies of the acquisition system over time, including both in-phase and quadrature components from the AEM acquisition system for each flightline.

used to estimate if there is likely to be enough signal for a repeat AEM to be useful.

3.2. Estimated parameters

The optimization ran for 250 iterations for 15 (3D-VDG simulated) years per iteration, taking on average five hours per iteration and ~2 months to complete on a standard desktop PC with four processing cores. The 3D-VDG model simulation was by far the most computationally intensive step, with the geophysical forward modelling, inversion, 3D interpolation and petrophysical transforms step only taking around half an hour in total per iteration.

The optimization results at each iteration are highlighted in Fig. 5, as the K_h/K_v ratio was kept constant only the K_h values are shown for the aquifers and aquitards.

Here it is apparent that there were two local minima: (1) between iterations 20 – 50 and (2) between 100 – 170, both of which were successfully avoided by the algorithm. Predictably changes in RMSE correlated well to changes in model parameters and showed that the steps between each iteration were appropriately sized and generally

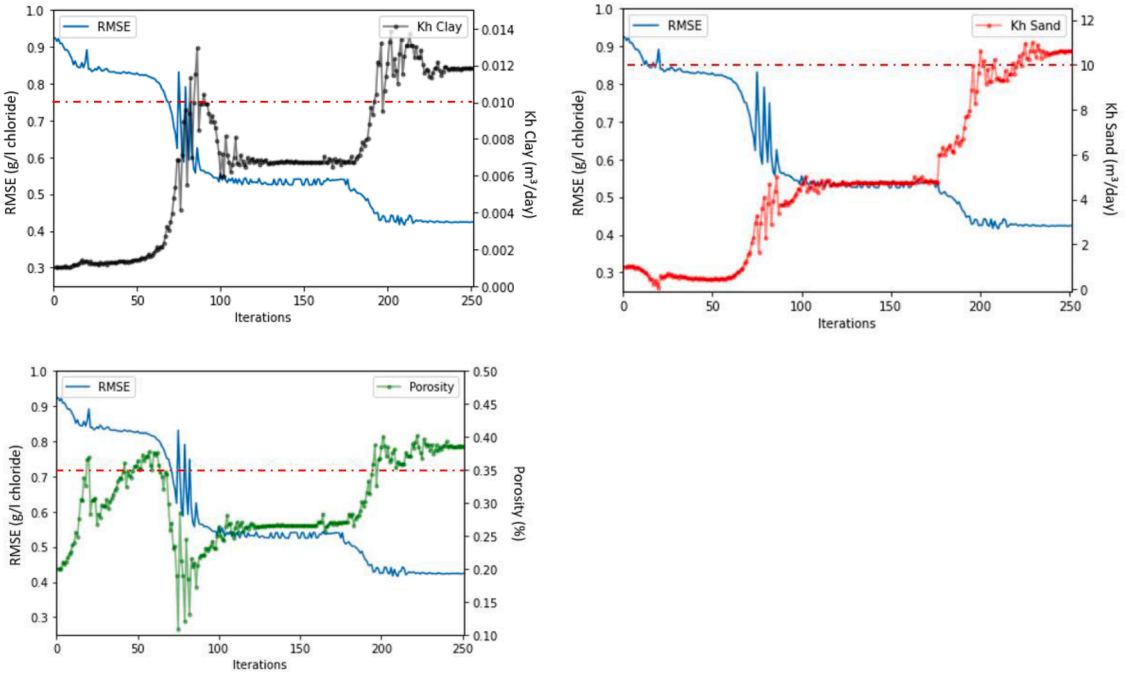

Fig. 5. RMSE (in g Cl^-/l) for each predicted model parameter over each iteration. Top left: predicted K_h clay (or aquitard) in m^3/day. Top right: predicted K_h cand (or aquifer) in m/day. Bottom left: predicted porosity (%). Red line indicates the real, target value.

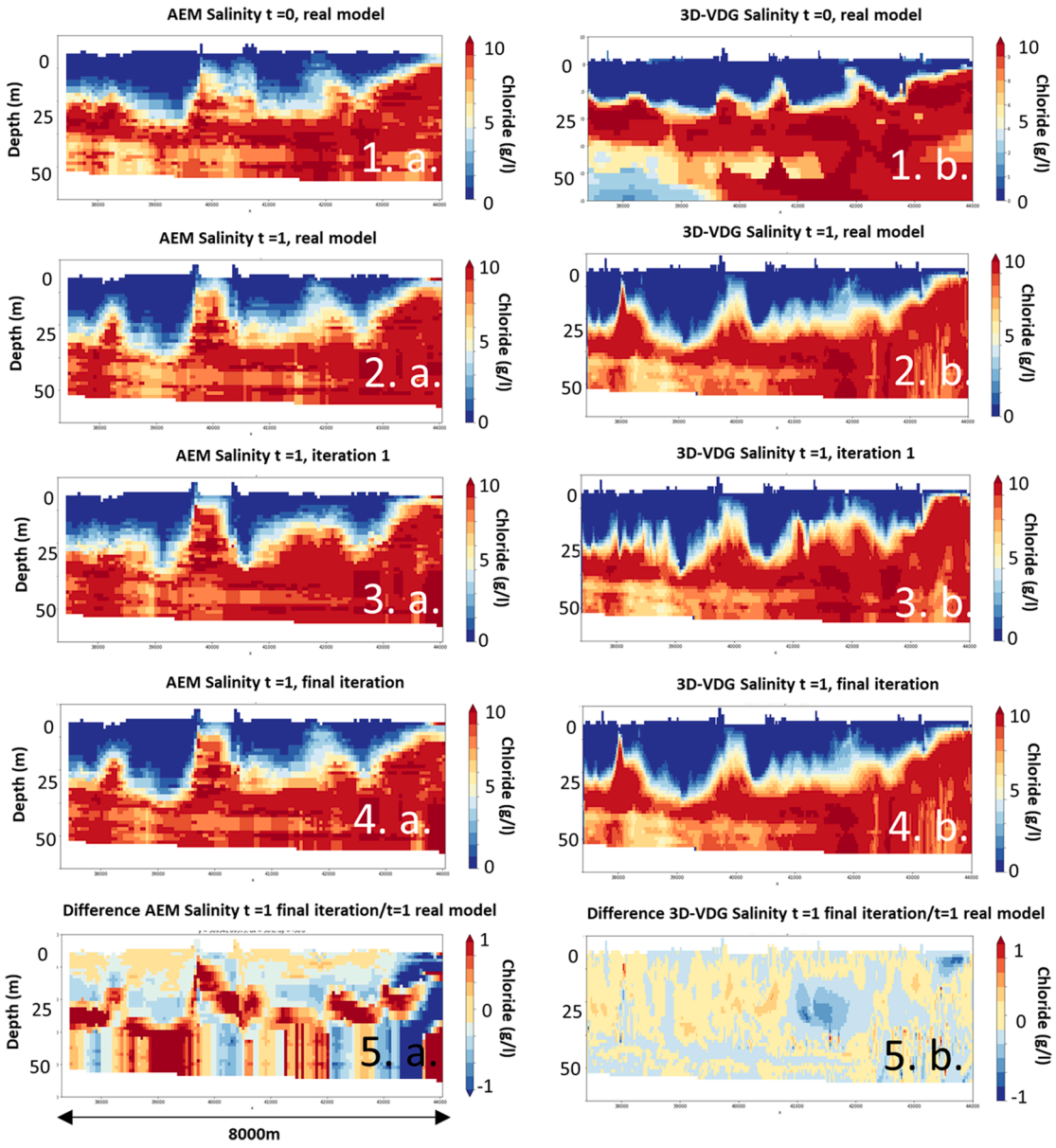

Fig. 6. AEM (left column) and 3D-VDG (right column) model results at t1 and initial salinity at t0. Rows 1 and 2 illustrate the 'real' model salinities at t0 and t1 respectively, therefore show our synthetic realities. Row 3 is the optimization result at the first iteration and the 4th row is the final optimization result at the final iteration. The last (5th) row is the difference between the final iteration and the synthetic reality. The section location is shown in Fig. 7 with the red line.

Table 4
The optimization results showing the values of initial, actual and predicted model parameters.

Parameter	Initial Estimate	Actual Value	Predicted Value (difference actual)
K_h Aquifer (m/day)	1	10	10.63291 (0.63291)
K_v Aquifer (m/day)	0.3	3	3.312433 (0.312433)
K_h Aquitard (m/day)	0.001	0.01	0.011838 (0.001838)
K_v Aquitard (m/day)	0.0005	0.005	0.005831 (0.000831)
Porosity	0.1	0.35	0.386181 (0.036181)

sensitive to the objective function. This is despite the fact that smaller changes in chloride distributions were *not* resolved as a result of the AEM simulation, the effect of which is highlighted in Fig. 6.

Quantitative results based on the final iteration (Table 4), suggest that each of the parameters were either successfully predicted or were improved considerably over the course of the optimization.

3.3. Estimated chloride distributions

Qualitative results of chloride distributions at t_1 are presented in Fig. 6, showing the synthetic reality on row 1.a. and 1.b. for the AEM salinity and 3D-VDG models respectively, followed by the results of the optimization, with the results of the first iteration on row 2, the last iteration on row 3 and the difference between the last iteration and the synthetic reality in row 4.

Comparing the chloride distributions between the AEM and the 3D-VDG models in general (columns 'a' and 'b' respectively), it is clear that the AEM simulation successfully mapped the locations of larger features such as upconing of saline groundwater and freshwater lenses. Smaller features (~< 200 m across) were not successfully resolved given the

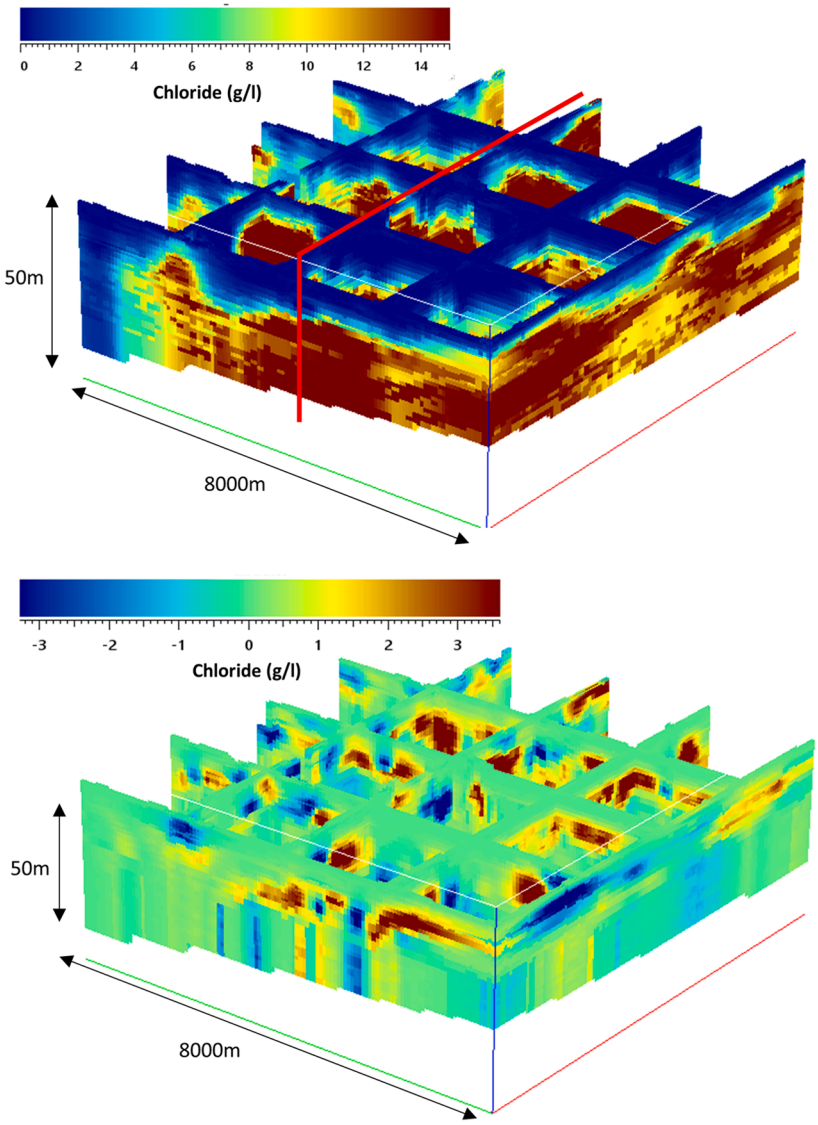

Fig. 7. 3D view of estimated simulated chloride distributions. Top: Final estimated AEM chloride distribution. Bottom: Differences between the first and final iteration AEM chloride distributions, highlighted zones that were updated by the optimization process.

footprint of the AEM system and the loss of resolution during the 3D interpolation of ECb values. In these areas the features have been smoothed out – effectively creating a vertically thicker brackish zone instead. It was also observed that the optimization successfully managed to recreate the synthetic realities' chloride distribution by the final iteration. The difference between the AEM synthetic reality (Fig. 6.1a) and the AEM final iteration (Fig. 6.3a) is larger than the differences between that of the 3D-VDG models. This is likely due to the 5% noise added in the geophysical modelling step and appears to cause uncertainty regarding the location of the fresh-saline interface. Despite this error, the 3D-VDG model was able to dynamically downscale the smoothed features observed in the AEM surveys.

Fig. 7 shows a 3D image of the final estimated AEM chloride distribution and the differences between the initial and final iteration thereof. The observed differences in salinity clearly show the zones where the chloride distribution was updated by the calibration process.

4. Discussion

Given the exploratory nature of this study, several necessary simplifications were made. As a result of these simplifications, in the following we will first discuss sources of uncertainty and their potential effects on our results, followed by a discussion of the optimization method. Finally, we mention thoughts on practicalities followed by potential for further research.

In this twin-experiment, we assumed that the synthetic model correctly describes reality – this assumption applies to the physics of the simulated AEM survey itself, as well as the magnitude of groundwater transport over time based on the 3D-VDG model. In the case of the AEM survey, we assumed that the chloride distributions were mapped with similar physical limitations to an actual survey. A major cause of this uncertainty is that we used a 1D geophysical forward and inverse modelling tool for a 3D problem (Auken et al., 2005), effectively removing 3D effects on the signal. Although there are 3D AEM geophysical modelling tools available (e.g., Cox et al., 2012), it was found that using these tools would lead to considerably longer iteration times on an already computationally expensive task. Instead, we added 5% gaussian noise which is considered an upper estimate of noise (Siemon, 2012) as well as simulating a 100 m footprint at measurement location (Reid et al., 2006; Yin et al., 2014). These steps effectively tested the robustness of repeat AEM surveys while maintaining reasonable optimization run-times.

For the 3D-VDG model simulation, we sought a careful balance between a realistic model while ensuring that there was sufficient signal for the optimization to work with. Based on a combination of using real subsurface data and known parameters, which were taken from an applied study (Mulder et al., 2020) as well as the groundwater modelling experience of the authors – we feel that the model describes reality to an acceptable level for meaningful conclusions.

An additional source of uncertainty is that we assume knowledge of parameter values and locations of the other hydrogeological parameters, such as the interaction between groundwater and drainage via the so-called drain resistance and the locations of aquitards and aquifers. We suggest that a simple way to examine the effect of keeping unknown parameter values constant would be to add noise to those that are not part of the optimization – where permitted deviations could be based on known uncertainty levels. The same could be said for the spatial distribution of clay and sand units, allowing the locations thereof to change based on given noise thresholds. The results of implementing this could then be used to determine quantitively the effect of these assumptions. Ideally, all uncertainties should have been included in the optimization as a fully heterogeneous 3D model. In this study, however, we chose to keep our method simple owing in part to the already high computational burden (discussed below) as well the fact that this is presented as a proof-of-concept – thus further complexity is considered subject for further study.

Besides correctly describing reality – uncertainty exists in both the type of geophysical inversion used, as well as the petrophysical transformation (i.e. to transform from ECb to salinity and vice-versa). Recent research highlights this, where it was found that the petrophysical transformation introduced the most uncertainty – and that overall incorrect handling of these two features can result in the mapping of an overly thick brackish zone (González-Quirós and Comte, 2020). The deterministic method used here suffers from non-uniqueness – where an infinite number of models can explain the data. In these cases regularization constrains the inversion, typically resulting in smooth models (Arsenin, 1979; Constable, 1987). One way to explore this effect is stochastic inversion, where a prior model is used instead of regularization (e.g. Minsley, 2011; Minsley et al., 2020). In this study we used a single inversion method as a necessity, given the computational burden of stochastic inversion. Furthermore, in this synthetic study we assume that the lithology is known – and that we estimate the properties of only the high and low permeability sediments. In real applications the efficacy of the AEM system for mapping similar shallow fresh-saline groundwater distributions, using the same geophysical inversion method, was quantitatively validated recently in Delsman et al. (2018). As a result, we feel that on balance our approach was valid for this study.

With the petrophysical model, we settled on the simpler apparent FF without using surface conductivities for a number of reasons. First, these values were derived from an actual, local field-study, and thus offered a good, realistic approximation for the study area. Second, lithologies such as peat and clay that could introduce error were only present as 1.4 and 6.2% of the total model volume respectively. As a result, we felt that additional uncertainty introduced when finding appropriate values for surface conductivity negated the use of local, representative data. It is however recommended that this step is taken with care in other use cases, given the propensity for incorrectly used petrophysical models to introduce non-physical error into hydrogeophysical models (González-Quirós and Comte, 2020). The ECb gradient is strongly controlled by fresh-saline groundwater contrasts – an effect also observed clearly in local ECb ground measurements. As such, despite potential error introduced in the petrophysical transformation and inversion, the relative magnitude of signal changes over time were considered sufficient to drive the optimization and were a good enough approximation for our purposes.

Overall, as the time-lapse approach presented here is new, we recommend that future research focusses on a global uncertainty analysis. Having a better quantitative grasp on what this means for practical mapping outcomes would be a useful step and potentially highlight methods to reduce uncertainty, for example the use of in-situ salinity data. For the purposes of this study however, we feel that the potential use of repeated airborne surveys was effectively proven given the highly realistic nature of our 3-D synthetic model.

The downhill-simplex optimization method used here (Gao and Han, 2012; Nelder and Mead, 1965) was selected for its simplicity and ability to handle highly-dimensional problems. Despite the successes of using the method in this study, in a practical (rather than exploratory) setting – we suggest that other methods are considered. This is recommended for two reasons: (1) the optimization was impractically slow to find a solution, and (2) the addition of other parameters would increase the likelihood of the downhill-simplex arriving at a local-minimum, especially given its sensitivity to the choice of initial guesses (Wang and Shoup, 2011). As the 3D-VDG model computation step cost ~5 h per iteration, one *could* simply run this step externally on large computational clusters using iMOD-SEAWAT, which utilizes distributed memory parallelization for faster computation times (Verkaik et al., 2021). In a practical setting however, we suggest fully parallelizing the optimization itself, using methods such as evolutionary algorithms (Brauer et al., 2002; Mühlenbein et al., 1991) and parallel Bayesian optimization (e.g. González et al., 2015; Kandasamy et al., 2017) where function evaluations can be done in parallel rather than sequentially. The latter approach has been successfully used in hydrocarbon reservoir modelling (e.g. Abdollahzadeh et al., 2011), where similar to the optimization used in this study, inverse problems are solved that require multiple flow-simulations, which are more computationally expensive compared to our problem. We consider the implementation of this an important avenue for future research given the possibility to parameterize fully heterogeneous models.

Finally, while the results of this research highlight the usefulness of two AEM surveys in time, we find it necessary to discuss these results against 3D hydrogeological inverse models that utilize different data configurations – for example a single AEM survey, or even multiple sources of in-situ head and salinity data.

Unlike this study, in these cases there isn't a complete picture of a groundwater state at two time intervals in 3D. As a result, an inverse modelling routine relies on a conceptualized version of the past based on prior knowledge, followed by a history matching routine until the chloride distribution is matched with acceptable accuracy to available data. This has the disadvantage that, owing to the large inertia of fresh-salt groundwater systems, simulations have to start far back in the past, sometimes hundreds to thousands of years back (Meyer et al., 2019; Delsman et al., 2014). Apart from being highly computationally expensive (in practice requiring) massively parallel computing, it also requires knowledge of boundary conditions from the distance past, adding considerable uncertainty and requiring extensive research. Nevertheless, we believe that a quantitative comparison between history matching to a single AEM survey and optimizing between two in a similar experiment would be useful as future research.

5. Conclusions

Using a twin-experiment involving two highly detailed synthetic realities and simulated airborne electromagnetic (AEM) surveys, it was successfully demonstrated that it is possible to jointly estimate groundwater salinity and hydrogeological parameters. In a real application, this could be achieved using a combination of two AEM surveys (flown across the same area over two periods in time) and a variable density groundwater flow and salt transport (3D-VDG) model. By coupling AEM and 3D-VDG models using geophysical forward modelling methods, it was shown that two AEM surveys are sensitive to changing groundwater chloride distributions over time - despite a significant loss of resolution as a result of the survey process itself. In doing so, it was also demonstrated that the time needed for chloride movements to be sensitive to AEM can be attained quantitatively. Given the knowledge of

sensitivities, it followed that an optimization method could be used to recover hydrogeological properties using 3D-VDG. With this in mind, a simple optimization process was implemented to resolve hydrogeological parameters of interest, while at the same time producing a physically consistent estimate of the chloride distribution at higher spatial resolution then the AEM surveys.

CRediT authorship contribution statement

Jude King: Conceptualization, Methodology, Writing – original draft, Writing – review & editing, Visualization. **Tobias Mulder:** Methodology, Writing – review & editing. **Gualbert Oude Essink:** Writing – review & editing, Methodology, Supervision. **Marc.F.P. Bierkens:** Supervision, Conceptualization, Methodology, Writing – review & editing, Writing – original draft.

Declaration of Competing Interest

The authors declare that they have no known competing financial interests or personal relationships that could have appeared to influence the work reported in this paper.

Acknowledgements

This research is financed by the Netherlands Organisation for Scientific Research (NWO), which is partly funded by the Ministry of Economic Affairs, and co-financed by the Netherlands Ministry of Infrastructure and Environment and partners of the Dutch Water Nexus consortium. Daniel Zamrsky and Joeri van Engelen are acknowledged for their helpful discussions about groundwater models.

Supplementary materials

Supplementary material associated with this article can be found, in the online version, at doi:10.1016/j.advwatres.2021.104118.

References

Abdollahzadeh, A., Reynolds, A., Christie, M., Corne, D., Davies, B., Williams, G., 2011. Bayesian optimization algorithm applied to uncertainty quantification. In: 73rd European Association of Geoscientists and Engineers Conference and Exhibition 2011: Unconventional Resources and the Role of Technology. Incorporating SPE EUROPEC 2011. Society of Petroleum Engineers, pp. 2317–2331. https://doi.org/10.2118/143290-ms.

Archie, G.E., 1942. The Electrical Resistivity Log as an Aid in Determining Some Reservoir Characteristics. Pet. Technol 54–62. https://doi.org/10.2118/942054-G.

Arsenin, A.N.T., 1979. Solutions of Ill-Posed Problems. Soc. Ind. Appl. Math. 21, 266–267.

Auken, E., Christiansen, A.V., Kirkegaard, C., Fiandaca, G., Schamper, C., Behroozmand, A.A., Binley, A., Nielsen, E., Effersø, F., Christensen, N.B., Sørensen, K., Foged, N., Vignoli, G., 2015a. An overview of a highly versatile forward and stable inverse algorithm for airborne, ground-based and borehole electromagnetic and electric data. Explor. Geophys. https://doi.org/10.1071/EG13097.

Auken, E., Christiansen, A.V., Jacobsen, B.H., Foged, N., Sørensen, K.I., 2005. Piecewise 1D laterally constrained inversion of resistivity data. Geophys. Prospect. 53, 497–506. https://doi.org/10.1111/j.1365-2478.2005.00486.x.

Auken, E., Christiansen, A.V., Jacobsen, L.H., Sørensen, K.I., 2008. A resolution study of buried valleys using laterally constrained inversion of TEM data. J. Appl. Geophys. 65, 10–20. https://doi.org/10.1016/j.jappgeo.2008.03.003.

Bauer-gottwein, P., Gondwe, B.N., Christiansen, L., Herckenrath, D., Kgotlhang, L., Zimmermann, S., Em, T., 2010. Hydrogeophysical exploration of three-dimensional salinity anomalies with the time-domain electromagnetic method (TDEM). J. Hydrol. 380, 318–329. https://doi.org/10.1016/j.jhydrol.2009.11.007.

Beaujean, J., Nguyen, F., Kemna, A., Antonsson, A., Engesgaard, P., 2014. Calibration of seawater intrusion models: inverse parameter estimation using surface electrical resistivity tomography and borehole data. Water Resour. Res. https://doi.org/10.1002/2013WR014020.

Berendsen, H.J.A., 2005. The Rhine-Meuse delta at a glance. In: 8th International Conference on Fluvial Sedimentology https://doi.org/ISBN-number: 90-77079-13-0.

Binley, A., Hubbard, S.S., Huisman, J.A., Revil, A., Robinson, D.A., Singha, K., Slater, L. D., 2015. The emergence of hydrogeophysics for improved understanding of subsurface processes over multiple scales. Water Resour. Res. 51, 3837–3866. https://doi.org/10.1002/2015WR017016.

Brauer, M.J., Holder, M.T., Dries, L.A., Zwickl, D.J., Lewis, P.O., Hillis, D.M., 2002. Genetic algorithms and parallel processing in maximum-likelihood phylogeny inference. Mol. Biol. Evol. 19, 1717–1726. https://doi.org/10.1093/oxfordjournals.molbev.a003994.

Carrera, J., Alcolea, A., Medina, A., Hidalgo, J., Slooten, L.J., 2005. Inverse problem in hydrogeology. Hydrogeol. J. https://doi.org/10.1007/s10040-004-0404-7.

Carrera, J., Hidalgo, J.J., Slooten, L.J., Vázquez-Suñé, E., 2010. Computational and conceptual issues in the calibration of seawater intrusion models. Hydrogeol. J. https://doi.org/10.1007/s10040-009-0524-1.

Chongo, M., Christiansen, A.V., Tembo, A., Banda, K.E., Nyambe, I.A., Larsen, F., Bauer-Gottwein, P., 2015. Airborne and ground-based transient electromagnetic mapping of groundwater salinity in the Machile-Zambezi Basin, southwestern Zambia. Near Surf. Geophys. 13, 383–395. https://doi.org/10.3997/1873-0604.2015024.

Cobaner, M., Yurtal, R., Dogan, A., Motz, L.H., 2012. Three dimensional simulation of seawater intrusion in coastal aquifers: a case study in the Goksu Deltaic Plain. J. Hydrol. 464–465, 262–280. https://doi.org/10.1016/J.JHYDROL.2012.07.022.

Constable, S.C., 1987. Occam's inversion: a practical algorithm for generating smooth models from electromagnetic sounding data. Geophysics 52, 289. https://doi.org/10.1190/1.1442303.

Cox, L.H., Wilson, G.A., Zhdanov, M.S., 2012. 3D inversion of airborne electromagnetic data. Geophysics 77, WB59–WB69. https://doi.org/10.1190/geo2011-0370.1.

De Louw, P.G.B., Eeman, S., Siemon, B., Voortman, B.R., Gunnink, J., Van Baaren, E.S., Oude Essink, G.H.P., 2011a. Shallow rainwater lenses in deltaic areas with saline seepage. Hydrol. Earth Syst. Sci. 15, 3659–3678. https://doi.org/10.5194/hess-15-3659-2011.

Delsman, J.R., Hu-A-Ng, K.R.M.R.M., Vos, P.C.C., De Louw, P.G.B., Oude Essink, G.H.P., Stuyfzand, P.J.P.J.J., Bierkens, M.F.P., 2014. Paleo-modeling of coastal saltwater intrusion during the Holocene: an application to the Netherlands. Hydrol. Earth Syst. Sci. 18, 3891–3905. https://doi.org/10.5194/hess-18-3891-2014.

Delsman, J.R., Van Baaren, E.S., Siemon, B., Dabekaussen, W., Karaoulis, M.C., Pauw, P. S., Vermaas, T., Bootsma, H., De Louw, P.G.B., Gunnink, J.L., Wim Dubelaar, C., Menkovic, A., Steuer, A., Meyer, U., Revil, A., Oude Essink, G.H.P., 2018. Large-scale, probabilistic salinity mapping using airborne electromagnetics for groundwater management in Zeeland, the Netherlands. Environ. Res. Lett. 13, 084011 https://doi.org/10.1088/1748-9326/aad19e.

Dillon, P., 2005. Future management of aquifer recharge. Hydrogeol. J. 131 (13), 313–316. https://doi.org/10.1007/S10040-004-0413-6, 2005.

Doherty, J., 2010. PEST: Model-Independent Parameter Estimation, User Manual, 5th Edition. PEST Man, p. 279. 5th Editio.

Faneca Sànchez, M., Gunnink, J.L., Van Baaren, E.S., Oude Essink, G.H.P., Siemon, B., Auken, E., Elderhorst, W., De Louw, P.G.B., 2012. Modelling climate change effects on a dutch coastal groundwater system using airborne electromagnetic measurements. Hydrol. Earth Syst. Sci. 16, 4499–4516. https://doi.org/10.5194/hess-16-4499-2012.

Farquharson, C.G., Oldenburg, D.W., Routh, P.S., 2003. Simultaneous 1D inversion of loop–loop electromagnetic data for magnetic susceptibility and electrical conductivity. Geophysics 68, 1857. https://doi.org/10.1190/1.1635038.

Fitterman, D.V., Deszcz-Pan, M., 2001. Saltwater Intrusion in Everglades National Park, Florida Measured by Airborne Electromagnetic Surveys.

Foged, N., Marker, P.A., Christansen, A.V., Bauer-Gottwein, P., Jørgensen, F., Høyer, A. S., Auken, E., 2014. Large-scale 3-D modeling by integration of resistivity models and borehole data through inversion. Hydrol. Earth Syst. Sci. 18, 4349–4362. https://doi.org/10.5194/HESS-18-4349-2014.

Gao, F., Han, L., 2012. Implementing the Nelder-Mead simplex algorithm with adaptive parameters. Comput. Optim. Appl. 51, 259–277. https://doi.org/10.1007/s10589-010-9329-3.

Goes, B.J.M., Oude Essink, G.H.P., Vernes, R.W., Sergi, F., 2009. Estimating the depth of fresh and brackish groundwater in a predominantly saline region using geophysical and hydrological methods, zeeland, the netherlands. Near Surf. Geophys. 7, 401–412. https://doi.org/10.3997/1873-0604.2009048.

Gomaa, S.M., Hassan, T.M., Helal, E., 2021. Assessment of seawater intrusion under different pumping scenarios in Moghra aquifer. Egypt. Sci. Total Environ. 781, 146710 https://doi.org/10.1016/J.SCITOTENV.2021.146710.

González-quirós, A., Comte, J., 2020. Advances in Water Resources Relative importance of conceptual and computational errors when delineating saltwater intrusion from resistivity inverse models in heterogeneous coastal aquifers. Adv. Water Resour. 144, 103695 https://doi.org/10.1016/j.advwatres.2020.103695.

González-Quirós, A., Comte, J.C., 2021. Hydrogeophysical model calibration and uncertainty analysis via full integration of PEST/PEST++ and COMSOL. Environ. Model. Softw. 145, 105183 https://doi.org/10.1016/J.ENVSOFT.2021.105183.

González, J., Dai, Z., Hennig, P., Lawrence, N.D., 2015. Batch Bayesian Optimization via Local Penalization. In: Proc. 19th Int. Conf. Artif. Intell. Stat. AISTATS, pp. 648–657, 2016.

Gossel, W., Sefelnasr, A., Wycisk, P., 2010. Modèelisation d'une paléeo-intrusion d'eau saléee dans la partie Nord du Systèeme Aquifèere Nubien, Nord-Est de l'Afrique. Hydrogeol. J. 18, 1447–1463. https://doi.org/10.1007/s10040-010-0597-x.

Green, A., Lane, R., 2013. Estimating Noise Levels in AEM Data. ASEG Ext. Abstr. 1–5. https://doi.org/10.1071/aseg2003ab093, 2003.

Gunnink, J.L., Bosch, J.H.A., Siemon, B., Roth, B., Auken, E., 2012. Combining ground-based and airborne em through Artificial Neural Networks for modelling glacial till under saline groundwater conditions. Hydrol. Earth Syst. Sci. 16, 3061–3074. https://doi.org/10.5194/hess-16-3061-2012.

Herckenrath, D., Fiandaca, G., Auken, E., Bauer-Gottwein, P., 2013. Sequential and joint hydrogeophysical inversion using a field-scale groundwater model with ERT and TDEM data. Hydrol. Earth Syst. Sci. 17, 4043–4060. https://doi.org/10.5194/hess-17-4043-2013.

Hinnell, A.C., Ferr, T.P.A., Vrugt, J.A., Huisman, J.A., Moysey, S., Rings, J., Kowalsky, M. B., 2010. Improved extraction of hydrologic information from geophysical data through coupled hydrogeophysical inversion. Water Resour. Res. 46, 1–14. https://doi.org/10.1029/2008WR007060.

Høyer, A.S., Jørgensen, F., Sandersen, P.B.E., Viezzoli, A., Møller, I., 2015. 3D geological modelling of a complex buried-valley network delineated from borehole and AEM data. J. Appl. Geophys. 122, 94–102. https://doi.org/10.1016/j.jappgeo.2015.09.004.

Huang, H., Cogbill, A., 2006. Repeatability study of helicopter-borne electromagnetic data. Geophysics 71, G285–G290. https://doi.org/10.1190/1.2353797.

Stafleu, J., Maljers, D., Gunnink, J.L., 2011. 3D modelling of the shallow subsurface of Zeeland, the Netherlands. Netherlands J. Geosci. 16, 5647. https://doi.org/10.5242/iamg.2011.0076.

Johnston, D.H., 2013. Practical Applications of Time-lapse Seismic Data. Pract. Appl. Time-lapse Seism. Data. https://doi.org/10.1190/1.9781560803126.

Jørgensen, F., Scheer, W., Thomsen, S., Sonnenborg, T.O., Hinsby, K., Wiederhold, H., Schamper, C., Burschil, T., Roth, B., Kirsch, R., Auken, E., 2012. Transboundary geophysical mapping of geological elements and salinity distribution critical for the assessment of future sea water intrusion in response to sea level rise. Hydrol. Earth Syst. Sci. 16, 1845–1862. https://doi.org/10.5194/hess-16-1845-2012.

Kandasamy, K., Krishnamurthy, A., Schneider, J., Poczos, B., 2017. Asynchronous Parallel Bayesian Optimisation via Thompson Sampling.

Karaoulis, M.C., Kim, J.H., Tsourlos, P.I., 2011. 4D active time constrained resistivity inversion. undefined 73, 25–34. https://doi.org/10.1016/J.JAPPGEO.2010.11.002.

King, J., King, J., Oude Essink, G., Oude Essink, G., Karaoulis, M., Bierkens, M.F.P., Bierkens, M.F.P., 2020. A practical quantification of error sources in regional-scale airborne groundwater salinity mapping. Environ. Res. Lett. 15 https://doi.org/10.1088/1748-9326/ab7b23.

King, J., Oude Essink, G., Karaolis, M., Siemon, B., Bierkens, M.F.P., 2018. Quantifying Geophysical Inversion Uncertainty Using Airborne Frequency Domain Electromagnetic Data—Applied at the Province of Zeeland, the Netherlands. Water Resour. Res. 54, 8420–8441. https://doi.org/10.1029/2018WR023165.

Kirkegaard, C., Sonnenborg, T.O., Auken, E., Jørgensen, F., 2011. Salinity Distribution in Heterogeneous Coastal Aquifers Mapped by Airborne Electromagnetics. Vadose Zo. J. 10, 125. https://doi.org/10.2136/vzj2010.0038.

Langevin, C.D., Thorne Jr, D.T., Dausman, A.M., Sukop, M.C., Guo, W., 2007. SEAWAT Version 4: a Computer Program for Simulation of Multi-Species Solute and Heat Transport. U.S. Geol. Surv. Tech. Methods B. 6, 39.

Mabrouk, M., Jonoski, A., Oude Essink, G.H.P., Uhlenbrook, S., 2019. Assessing the Fresh-Saline Groundwater Distribution in the Nile Delta Aquifer Using a 3D Variable-Density Groundwater Flow Model. https://doi.org/10.3390/w11091946.

Meyer, R., Engesgaard, P., Sonnenborg, T.O., 2019. Origin and Dynamics of Saltwater Intrusion in a Regional Aquifer: combining 3-D Saltwater Modeling With Geophysical and Geochemical Data. Water Resour. Res. 55, 1792–1813. https://doi.org/10.1029/2018WR023624.

Michael, H.A., Voss, C.I., Gossel, W., Sefelnasr, A., Wycisk, P., Nocchi, M., Salleolini, M., 2009. A 3D density-dependent model for assessment and optimization of water management policy in a coastal carbonate aquifer exploited for water supply and fish farming. Hydrogeol. J. 18, 200–218. https://doi.org/10.1007/s10040-010-0597-x.

Minsley, B.J., 2011. A trans-dimensional Bayesian Markov chain Monte Carlo algorithm for model assessment using frequency-domain electromagnetic data. Geophys. J. Int. 187, 252–272. https://doi.org/10.1111/j.1365-246X.2011.05165.x.

Minsley, B.J., Foks, N.L., Bedrosian, P.A., 2020. Quantifying model structural uncertainty using airborne electromagnetic data. Geophys. J. Int. 224, 590–607. https://doi.org/10.1093/GJI/GGAA393.

Mühlenbein, H., Schomisch, M., Born, J., 1991. The parallel genetic algorithm as function optimizer. Parallel Comput 17, 619–632. https://doi.org/10.1016/S0167-8191(05)80052-3.

Nelder, J.A., Mead, R., 1965. A Simplex Method for Function Minimization. Comput. J. 7, 308–313. https://doi.org/10.1093/comjnl/7.4.308.

Nocchi, M., Salleolini, M., 2013. A 3D density-dependent model for assessment and optimization of water management policy in a coastal carbonate aquifer exploited for water supply and fish farming. J. Hydrol. 492, 200–218. https://doi.org/10.1016/j.jhydrol.2013.03.048.

Oude Essink, G.H.P., Van Baaren, E.S., De Louw, P.G.B., 2010. Effects of climate change on coastal groundwater systems: a modeling study in the Netherlands. Water Resour. Res. 46, 1–16. https://doi.org/10.1029/2009WR008719.

Pauw, P.S., van Baaren, E.S., Visser, M., de Louw, P.G.B., Essink, G.H.P.O., 2015. Increasing a freshwater lens below a creek ridge using a controlled artificial recharge and drainage system: a case study in the Netherlands. Hydrogeol. J. 23, 1415–1430. https://doi.org/10.1007/s10040-015-1264-z.

Rahman, M.A., Zhao, Q., Wiederhold, H., Skibbe, N., Eva González, Deus, N., Siemon, Bernhard, Kirsch, Reinhard, Elbracht, J., González, E., Siemon, B., Kirsch, R., n.d. Coastal Groundwater systems: Mapping Chloride Distribution from Borehole and Geophysical Data. Grundwasser. https://doi.org/10.1007/s00767-021-00475-1.

Reid, J.E., Pfaffling, A., Vrbancich, J., 2006. Airborne electromagnetic footprints in 1D earths. Geophysics 71. https://doi.org/10.1190/1.2187756.

Revil, A., Coperey, A., Shao, Z., Florsch, N., Fabricius, I.L., Deng, Y., Delsman, J.R., Pauw, P.S., Karaoulis, M., de Louw, P.G.B., van Baaren, E.S., Dabekaussen, W., Menkovic, A., Gunnink, J.L., 2017. Complex conductivity of soils. Water Resour. Res. 53, 7121–7147. https://doi.org/10.1002/2017WR020655.

Revil, A., Glover, P.W.J., 1998. Nature of surface electrical conductivity sandstones, and clays in natural sands. Geophys. Res. Lett. 25, 691–694.

Siemon, B., 2012. Accurate 1D forward and inverse modeling of high-frequency helicopter-borne electromagnetic data. Geophysics 77, WB71. https://doi.org/10.1190/geo2011-0371.1.

Simmons, C.T., Bauer-Gottwein, P., Graf, T., Kinzelbach, W., Kooi, H., Li, L., Post, V.E.A., Prommer, H., Therrien, R., Voss, C.I., Ward, J., Werner, A.D., 2010. Variable density groundwater flow: from modelling to applications. J Chem Inf Model. https://doi.org/10.1017/CBO9781107415324.004.

Steklova, K., Haber, E., 2015. Joint Hydrogeophysical Inversion : state Estimation for Seawater Intrusion Models in 3D. J. Hydrol. https://doi.org/10.1007/s10596-016-9595-y.

Van Engelen, J., Verkaik, J., King, J., Nofal, E.R., Bierkens, M.F.P., Oude Essink, G.H.P., 2019. A three-dimensional palaeohydrogeological reconstruction of the groundwater salinity distribution in the Nile Delta Aquifer. Hydrol. Earth Syst. Sci. 23 https://doi.org/10.5194/hess-23-5175-2019.

Vandevelde, D., Van Baaren, E., Delsman, J., Karaoulis, M., Oude Essink, G., De Louw, P., Vermaas, T., Pauw, P., De Kleine, M., Thofte, S., Teilmann, R., Walraevens, K., Van Camp, M., Dominique, H., Dabekaussen, W., Gunnink, J., Vandenbohede, A., 2018. Groundwater salinity mapping of the Belgian coastal zone to improve local freshwater storage availability. In: E3S Web Conf, 54. https://doi.org/10.1051/e3sconf/20185400040.

Verkaik, J., van Engelen, J., Huizer, S., Bierkens, M.F.P., Lin, H.X., Oude Essink, G.H.P., 2021. Distributed memory parallel computing of three-dimensional variable-density groundwater flow and salt transport. Adv. Water Resour. 154, 103976 https://doi.org/10.1016/j.advwatres.2021.103976.

Vest Christiansen, A., Auken, E., 2012. A global measure for depth of investigation. Geophysics 77, WB171. https://doi.org/10.1190/geo2011-0393.1.

Viezzoli, A., Auken, E., Munday, T., 2009. Spatially constrained inversion for quasi 3D modelling of airborne electromagnetic data an application for environmental assessment in the Lower Murray Region of South Australia. Explor. Geophys. 40, 173–183. https://doi.org/10.1071/EG08027.

Vignoli, G., Fiandaca, G., Christiansen, A.V., Kirkegaard, C., Auken, E., 2015. Sharp spatially constrained inversion with applications to transient electromagnetic data. Geophys. Prospect. 63, 243–255. https://doi.org/10.1111/1365-2478.12185.

Vos, P.C., 2015. Origin of the Dutch coastal landscape.

Wang, P.C., Shoup, T.E., 2011. Parameter sensitivity study of the Nelder-Mead Simplex Method. Adv. Eng. Softw. 42, 529–533. https://doi.org/10.1016/j.advengsoft.2011.04.004.

Waxman, M.H., Smits, L.J.M., 2003. Electrical Conductivities in Oil-Bearing Shaly Sands. SPE Repr. Ser. 8, 107–122. https://doi.org/10.2118/1863-a.

Werner, A.D., Bakker, M., Post, V.E.A., Vandenbohede, A., Lu, C., Ataie-Ashtiani, B., Simmons, C.T., Barry, D.A., 2013. Seawater intrusion processes, investigation and management: recent advances and future challenges. Adv. Water Resour. 51, 3–26. https://doi.org/10.1016/j.advwatres.2012.03.004.

Yin, C., Huang, X., Liu, Y., Cai, J., 2014. Footprint for frequency-domain airborne electromagnetic systems. Geophysics 79, E243–E254. https://doi.org/10.1190/geo2014-0007.1.

Zhou, sH., Gómez-hernández, J.J., Li, L., 2014. Advances in Water Resources Inverse methods in hydrogeology : evolution and recent trends. Adv. Water Resour. 63, 22–37. https://doi.org/10.1016/j.advwatres.2013.10.014.

Zuurbier, K.G., Kooiman, J.W., Groen, M.M.A., Maas, B., Stuyfzand, P.J., 2015. Enabling Successful Aquifer Storage and Recovery of Freshwater Using Horizontal Directional Drilled Wells in Coastal Aquifers. J. Hydrol. Eng. 20 https://doi.org/10.1061/(asce)he.1943-5584.0000990.